American Mineralogist, Volume 81, pages 61–66, 1996

Structure and crystal-field spectra of $Co_3Al_2(SiO_4)_3$ and $(Mg,Ni)_3Al_2(SiO_4)_3$ garnet

CHARLES R. ROSS II,* HANS KEPPLER, DANTE CANIL,† AND Hugh St. C. O'Neill‡

Bayerisches Geoinstitut, Universität Bayreuth, 95440 Bayreuth, Germany

ABSTRACT

Synthetic $Co_3Al_2(SiO_4)_3$ garnet and $(Mg,Ni)_3Al_2(SiO_4)_3$ garnet with Ni/(Ni + Mg) = 0.15–0.18 have been studied by single-crystal X-ray diffraction and optical spectroscopy. The X-ray data confirm that Co^{2+} and Ni^{2+} occupy the large distorted cubic (dodecahedral) site of the structure. Structure refinement indicates that the Ni^{2+} ion is probably displaced out of the center of this site and statically or dynamically disordered onto the 48*g* equipoint at $(1/8,y,1/4+y)$. This is consistent with the lattice constant of the Ni-bearing garnet of 11.4717(7) Å being significantly larger than the lattice constant of pyrope (11.459 Å), although the ionic radius of Ni^{2+} is usually smaller than that of Mg^{2+}. The lattice constant of $Co_3Al_2(SiO_4)_3$ garnet is 11.4597(2) Å. Because of the unusual coordination geometries of Ni^{2+} and Co^{2+}, the optical spectra of the garnets are fundamentally different from those of other Co^{2+}- and Ni^{2+}-bearing silicates. The following crystal-field parameters were estimated from spectroscopic data: crystal-field splitting $\Delta = 4430\ cm^{-1}$ (Co^{2+}) and 4210 cm^{-1} (Ni^{2+}); Racah parameter $B = 890\ cm^{-1}$ (Co^{2+}) and 1080 cm^{-1} (Ni^{2+}). These data yield an exceptionally low crystal-field stabilization energy (CFSE) of Ni^{2+} in garnet of 3370 cm^{-1}, which explains the very low Ni contents of garnets in equilibrium with olivine. The CFSE of Co^{2+} in garnet of 5320 cm^{-1} is similar to values for pyroxenes and olivine. Therefore, the partition coefficient of Co^{2+} between these phases should be close to unity, as is observed.

INTRODUCTION

The partitioning of Ni between olivine and pyrope garnet is strongly temperature dependent (Griffin et al. 1989; Canil 1994) and can be used as a geothermometer. Because the garnet-olivine partition coefficient of Ni is very low and the Ni content of mantle olivine is rather uniform, a temperature estimate may be obtained by just measuring the Ni content of a garnet, e.g., of an inclusion in diamond. To understand the crystal chemistry of Ni and Co in the garnet structure, we performed an X-ray diffraction and optical spectroscopic study of synthetic $Co_3Al_2(SiO_4)_3$ and $(Mg,Ni)_3Al_2(SiO_4)_3$ garnet.

The most interesting aspect of the structure of the Ni^{2+}-bearing garnet is the fact that Ni^{2+} is considerably smaller than Mg^{2+}, which is the smallest of the cations commonly found in the dodecahedral site in aluminous garnets (Novak and Gibbs 1971). Indeed, Mg is so small relative to this site that it has been suggested that in pyrope $Mg_3Al_2(SiO_4)_3$ the Mg atom is not actually found at the 24*c* equipoint at (1/8, 0, 1/4), which defines the symmetry of the dodecahedral site, but is rather statically or dynamically disordered into the 48*g* equipoint at $(1/8,y,1/4+y)$. This disorder is consistent with the high degree of distortion of the thermal motion ellipsoid found for the dodecahedral site in pyrope; however, unequivocal evidence for this disorder has never been found. With the substitution of Ni on this site, the misfit of the cation and the site may become so great as to reveal this disorder unequivocally.

The dodecahedral site of garnet is a very unusual environment for Ni^{2+} and Co^{2+}, which are octahedrally coordinated in most silicates. Co^{2+} even occasionally enters tetrahedral sites, e.g., in staurolite (Burns 1993). Therefore, the optical spectra and crystal-field stabilization energies of Ni^{2+} and Co^{2+} in garnets are expected to be quite different from other silicates.

SYNTHESIS OF GARNETS

$Co_3Al_2(SiO_4)_3$ garnet was prepared from an oxide mixture in the presence of traces of water in a piston-cylinder apparatus at 45 kbar and 1100 °C for 16 h. The product was single-phase $Co_3Al_2(SiO_4)_3$ garnet.

Ni-bearing pyrope was synthesized in a sealed platinum capsule from a mixture of oxides with the bulk composition $Mg_2NiAl_3Si_4O_{12}$. Two wt% brucite was added as a source of water. Synthesis was conducted at 80 kbar and 1500 °C for 3 h in a multi-anvil apparatus. The experimental products were dominantly garnet with a molar ratio of Ni/(Ni + Mg) of 0.15–0.18. In addition, some

* Present address: Department of Chemistry, University of Nebraska, Lincoln, Nebraska 68588, U.S.A.

† Present address: School of Earth and Ocean Sciences, University of Victoria, Victoria, British Columbia V8W 2Y2, Canada.

‡ Present address: Research School of Earth Sciences, Australian National University, Canberra 2601, Australia.

0003–004X/96/0102–0061$05.00

TABLE 1. *R* factors (%) and structural parameters

Parameter	Co–end-member garnet	Ni-bearing garnet
R_m	2.2	2.9
R	1.7	2.2
R_w	2.6	2.7
N_{ref}	314	277
N_{par}	18	20
$y_{[8]}$	—	−0.0081(1)
x_O	0.0336(1)	0.0328(1)
y_O	0.0512(1)	0.0493(1)
z_O	0.6529(1)	0.6533(1)
x_{Ni}	—	0.150(2)

Ni-bearing olivine, nickel-aluminum-silicate spinel and quenched melt were present. The garnet grains used in the present study were unzoned and free of inclusions, according to microprobe analysis.

Both the Co–end-member garnet and Ni-bearing garnet samples had grain sizes of up to several hundred micrometers. The Co–end-member garnets are intensely purple in color. The color of the Ni-bearing garnets is between orange and pink.

EXPERIMENTAL METHODS

Single-crystal X-ray diffraction

Candidate crystals were selected and mounted on an Enraf-Nonius CAD4 diffractometer using graphite-monochromated Mo$K\alpha$ radiation ($K\alpha_1$ = 0.70930, $K\alpha_2$ = 0.71359 Å). The crystal quality was evaluated by examination of rotation photographs and the mapping of selected reflections in reciprocal space until a satisfactory crystal was found. After determination and refinement of the orientation matrix, one-sixteenth of reciprocal space ($h, k \geq 0, l \geq k$) to ($\sin\theta)/\lambda \approx 1.0$ ($\theta = 45°$) was collected in ω-2θ scan mode. The crystal alignment was checked after the collection of every 150 reflections, the intensity of standard reflections was checked every hour. After data collection, ψ-scan data were collected for the application of an empirical absorption correction.

The data were corrected for Lorentz and polarization effects, as well as for absorption. Symmetrically equivalent data were then averaged, with R_{merge} = 2.2 [$Co_3Al_2(SiO_4)_3$] or 2.9 [$(Mg,Ni)_3Al_2(SiO_4)_3$]. Structure factors were weighted using a modified Poisson weighting scheme that reduces the influence of intense reflections.

Optical spectroscopy

To record absorption spectra from 2500 to 27500 cm^{-1} (near infrared to near UV), doubly polished plates with a thickness of 32 μm were prepared from the garnets. Measurements were made using a Bruker IFS 120 HR infrared spectrometer equipped with a Bruker infrared microscope. The spot size of the beam was between 40 and 70 μm. From every sample, three spectra in different wavelength ranges (2500–10000, 9000–15000, and 12500–27500 cm^{-1}) were accumulated and merged to the final spectrum. The spectroscopic resolution was 4 cm^{-1} in the infrared and 8 cm^{-1} in the visible and UV range. Depending on the spectral range, different light sources (tungsten lamp or xenon arc lamp), beamsplitters (Si-coated CaF_2 or quartz), and detectors (narrow-band MCT or Si-diode) were used. Between 1000 and 5000 scans were accumulated for each spectrum.

RESULTS

Structure refinement

For each data set, two models were refined in space group $Ia\bar{3}d$. In the first model, the dodecahedral cation was assumed to be ordered on equipoint 24*c*, requiring a total of 16 structural parameters (O positional parameters and anisotropic displacement factors) in addition to a scale factor. For the second model, the dodecahedral cation was allowed to relax onto the 48*g* equipoint, requiring two additional parameters, i.e., the $y_{[8]}$ and $\beta_{12[8]}$ parameters. In addition, the Ni content of the dodecahedral site was refined for the Ni-bearing pyrope.

Model 1 resulted in acceptable *R* factors for both materials (although it was necessary to refine an extinction coefficient for the Co–end-member garnet). The vibrational ellipsoids of the dodecahedral site were large and distorted (particularly for the Ni-bearing garnet).

The refinement of the Co data using model 2 was somewhat unstable and resulted in no change in R_w. The refinement of the Ni data using model 2 resulted in a slight improvement in R_w (R_w = 0.027 for model 2, R_w = 0.029 for model 1). Although this improvement is slight, Hamilton's (1965) significance test indicated that it is highly significant, i.e., the disordered cation site is clearly a better model. According to Hamilton's test, the probability that model 2 is correct rather than model 1 is 99.5%.

The vibrational ellipsoid for the dodecahedral site in Ni-bearing pyrope is quite large and highly anisotropic even in model 2, although the distortion is more in line with the values found for the Co–end-member garnet. The displacement parameters are large for the dodecahedral site in both materials. The remaining displacement parameters for the Co–end-member garnet are generally in accordance with those reported for pyrope (Gibbs and Smith 1965; Novak and Gibbs 1971); however, all the displacement factors for the Ni-bearing pyrope are significantly larger than those found in pyrope or the Co–end-member garnet. This perhaps suggests that the structure is so uncomfortable (at ambient conditions) with Ni in the dodecahedral site that the entire structure is placed under considerable strain. This strain may be attributed to the misfit between the Ni atom and its site; if the dodecahedral site were perfectly rigid, then the only effect of substituting Ni for Mg would be (as indicated by this structure refinement) the relaxation of the Ni atoms off of the center of the site. Indeed, the dodecahedral site is not perfectly rigid, and so for those sites in which Ni is found, the coordinating O atoms shift to accommodate the requirements of bonding to the smaller cation. These shifts have two effects. The first is to increase the apparent displacement coefficient of O. The second is to trans-

TABLE 2. Anisotropic displacement parameters (β values $\times 10^5$)

β	Co-end-member garnet	Ni-bearing garnet
$11_{[8]}$	56(1)	113(4)
$22_{[8]}$	145(1)	309(3)
$12_{[8]}$	—	70(10)
$23_{[8]}$	77(3)	371(8)
$11_{[6]}$	45(2)	61(2)
$12_{[6]}$	1(4)	−1(4)
$11_{[4]}$	37(3)	60(3)
$22_{[4]}$	44(2)	68(2)
11_{O}	71(3)	95(3)
22_{O}	88(3)	120(3)
33_{O}	51(3)	82(3)
12_{O}	36(7)	36(7)
13_{O}	−31(7)	40(7)
23_{O}	−8(6)	−11(6)

Note: The form of the anisotropic displacement parameter for the garnet structure is $\exp(h^2\beta_{11} + k^2\beta_{22} + l^2\beta_{33} + hk\beta_{12} + hl\beta_{13} + kl\beta_{23})$. For the dodecahedral [8] site, $\beta_{22} = \beta_{33}$, $\beta_{12} = \beta_{13} = 0$; for the disordered dodecahedral site, in addition $\beta_{13} = -\beta_{12}$. For the octahedral [6] site, $\beta_{11} = \beta_{22} = \beta_{33}$, $\beta_{12} = \beta_{13} = \beta_{23}$. For the tetrahedral [4] site, $\beta_{22} = \beta_{33}$, $\beta_{12} = \beta_{13} = \beta_{23} = 0$.

TABLE 3. Bond lengths (Å) and distortion indices

	Co-end-member garnet	Ni-bearing garnet
	Dodecahedral site	
M-O (Å)	2.332 × 4	2.457 × 2
		2.245 × 2
M-O′ (Å)	2.211 × 4	2.225 × 2
		2.179 × 2
V (Å^3)	20.085	20.247
	Octahedral site	
M-O (Å)	1.887 × 6	1.889 × 6
V (Å^3)	8.949	8.965
q.e.	1.0013	1.0013
a.v.	4.58	4.61
	Tetrahedral site	
M-O (Å)	1.637 × 4	1.635 × 4
V (Å^3)	2.210	2.191
q.e.	1.0123	1.0154
a.v.	50.65	63.22

Note: q.e. = quadratic elongation, a.v. = angle variation; for definitions, see Hazen and Finger 1982. Bond lengths uncorrected for thermal motion.

fer strains through the densely packed garnet structure to the other structural elements and thus cause a general increase in the displacement coefficients.

Table 1 lists the final R factors and structural parameters, whereas Table 2 lists the final anisotropic displacement parameters. A listing of observed and final calculated structure factors may be obtained from the authors.

The unit-cell parameters were determined by centering a group of 18 high-angle reflections in four diffraction conditions (routine SET4 in Enraf-Nonius's data collection package) to eliminate alignment errors. The cell parameters, constrained to a cubic cell, were 11.4597(2) Å (Co) and 11.4717(7) Å (Ni). There was no significant evidence of deviation from cubic symmetry. It is interesting to note that the lattice constant of the Ni-bearing garnet is significantly larger than the lattice constant of pyrope (11.459 Å, Skinner 1956), although Ni^{2+} (ionic radius 0.690 Å, Shannon 1976) is smaller than Mg^{2+} (0.720 Å). This is consistent with the assumption of Ni^{2+} being disordered out of the center of the dodecahedral site. The lattice constant of the Co-end-member garnet is slightly larger than that of pyrope, as expected from the larger ionic radius of Co^{2+} (0.745 Å) in comparison with Mg^{2+}.

Table 3 lists the calculated bond lengths and distortion indices (compare Hazen and Finger 1982) for the two structures. Note that the Al-O and Si-O bond lengths are indifferent to the identity of the atom in the dodecahedral site. The structural data for the Co-end-member garnet are similar to those obtained by Ohashi et al. (1981).

Crystal-field spectra

Crystal-field spectra of the Co-end-member and Ni-bearing garnet are shown in Figures 1 and 2, and spectroscopic data are in Tables 4 and 5. In an ideal eightfold-coordinated cubic environment, the ground state of Co^{2+} is $^4A_{2g}(F)$. From this ground state, three spin-allowed transitions are expected to occur to the excited states $^4T_{2g}(F)$, $^4T_{1g}(F)$, and $^4T_{1g}(P)$. These transitions correspond to the three band systems centered at 4320, 8170, and 18300 cm^{-1} (Fig. 1, Table 4). Because of the orthorhombic site symmetry of the distorted cubic (dodecahedral) site in garnet, the degeneracy of the $^4T_{2g}(F)$, $^4T_{1g}(F)$, and $^4T_{1g}(P)$ terms is completely lifted, causing the splitting of each of three major absorption bands into three components. This splitting is clearly seen in Figure 1. In addition to site distortion, spin-orbit coupling may contribute to the observed fine structure (Stahl-Brada and Low 1959). The band system centered around 18300 cm^{-1} in the visible range also involves some spin-forbidden transitions to the $^2A_{2g}(G)$, $^2T_{1g}(D)$, and $^2E_g(G)$ states. A precise assignment of the band components is not possible. The weak feature at 22530 cm^{-1} is due to the transition $^4A_{2g}(F) \rightarrow {}^2T_{2g}(G)$. Attempts were made to more precisely locate individual band components by deconvoluting the spectra in Figures 1 and 2 into Gaussian peaks. However, a satisfactory fit of the experimental data could not be obtained using a physically meaningful number of individual band components. This is probably because of the intrinsic asymmetry of some bands.

If one treats the orthorhombic site symmetry as a slight perturbation of a cubic field, crystal-field parameters can be estimated from the barycenter of the three major band systems centered at 4320, 8170, and 18300 cm^{-1}. This yields a crystal-field splitting $\Delta = 4430$ cm^{-1} and a Racah parameter $B = 890$ cm^{-1} (Table 6). With these parameters, a satisfactory agreement between observed and predicted band positions can be obtained (Table 4). In the cubic approximation, the crystal-field stabilization energy (CFSE) of Co^{2+} is $= {}^6/_5\Delta = 5320$ cm^{-1}.

The ground state of Ni^{2+} in an ideal eightfold-coordinated cubic environment is $^3T_{1g}(F)$. Three spin-allowed transitions are expected to occur to the excited states

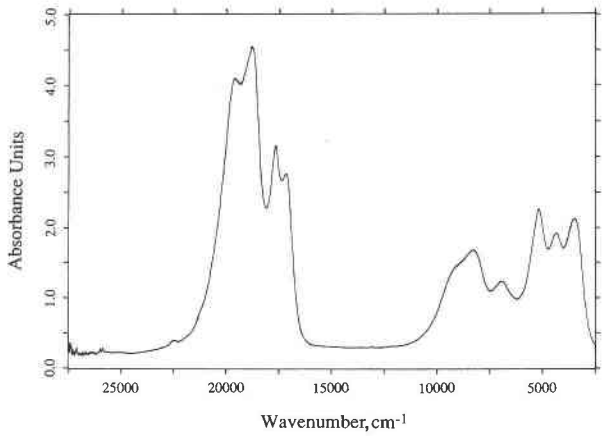

FIGURE 1. Crystal-field spectrum of $Co_3Al_2(SiO_4)_3$ garnet, renormalized to 100 μm thickness.

$^3T_{2g}(F)$, $^3A_{2g}(F)$, and $^3T_{1g}(P)$. The first two transitions are observed at 4070 and 6210 cm^{-1}. They do not show any splitting owing to the low site symmetry. However, the third band, centered around 20640 cm^{-1}, is clearly split into at least two components. A weak absorption feature at 13630 cm^{-1} is due to the spin-forbidden transition to the $^1E_g(D)$ and $^1T_{2g}(D)$ states. Estimated crystal-field parameters are $\Delta = 4210$ cm^{-1} and $B = 1080$ cm^{-1}; CFSE $= {}^4/_5\Delta = 3370$ cm^{-1} in the cubic-field approximation (Table 6). This simple cubic treatment, however, cannot satisfactorily account for the relative energies of the transitions $^3T_{1g}(F) \rightarrow {}^3T_{2g}(F)$ and $^3T_{1g}(F) \rightarrow {}^3A_{2g}(F)$. Because the slope of the energy of the $^3T_{2g}(F)$ and $^4A_{2g}(F)$ terms in the Tanabe-Sugano diagram is constant (Figgis 1966), the ratio of the two transition energies should be the same for any value of Δ or B. This ratio should be close to 2. The observed ratio, however, is 1.5. This cannot be explained by a simple cubic-field approximation and must be due to the low site symmetry, possibly combined with disordering between two sites.

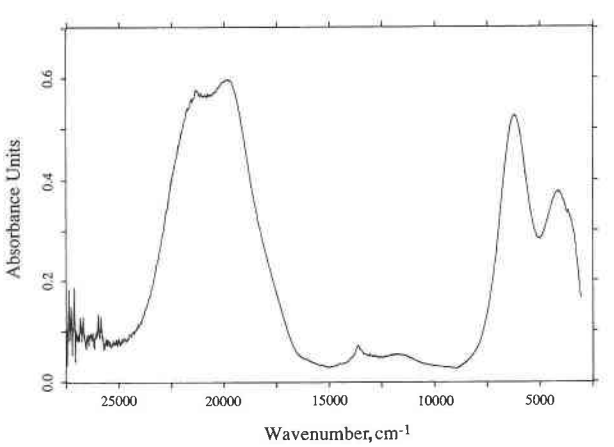

FIGURE 2. Crystal-field spectrum of $(Mg_{0.82}Ni_{0.18})_3Al_2(SiO_4)_3$ garnet, renormalized to 100 μm thickness.

TABLE 4. Crystal-field spectrum of $Co_3Al_2(SiO_4)_3$ garnet

Band position (cm^{-1})	ϵ [L/(mol·cm)]	Excited state	Barycenter of split bands (cm^{-1})	Calc. band position (cm^{-1})
3460	8.04			
4320	7.25	$^4T_{2g}(F)$	4320	4430
5170	8.57			
6910	4.64			
8300	6.34	$^4T_{1g}(F)$	8170	7690
9300 (shoulder)	5.13			
17140	10.38			
17650	11.89	$^4T_{1g}(P)$	18300	18900
18770	17.17			
19640	15.47			
22530	1.51	$^2T_{2g}(G)$		

Note: Term symbols for undistorted cubic environment are used. Ground state is $^4A_{2g}(F)$. Positions of the spin-allowed bands are calculated from the crystal-field parameters in Table 6; ϵ = molar extinction coefficient of Co in garnet as measured at the respective wavenumber.

GEOLOGICAL APPLICATIONS

Crystal-field stabilization energies can be used to predict the partitioning of trace elements between different phases (Burns 1993). The correct order of magnitude of partition coefficients can often be obtained by considering CFSE alone, at least for ions having high CFSE, such as Ni^{2+}, Co^{2+}, and Cr^{3+} in octahedral sites (Keppler 1992). For example, the CFSE of Ni^{2+} and Co^{2+} in glasses quenched from pressures up to 100 kbar have been used to predict the pressure dependence of the metal-silicate melt partition coefficients of these elements (Keppler and Rubie 1993); the predicted changes in the partition coefficients have recently been confirmed experimentally (Thibault and Walter 1995). At first sight, this may seem surprising because crystal-field stabilization usually accounts for only about 10–30% of the total bonding energy of an ion. There are two explanations, however, for the success of considerations of CFSE in the prediction of partition coefficients; one is based on simple electrostatic arguments, whereas the other stems from molecular orbital theory. A simple electrostatic model predicts that the magnitude of Δ, and therefore the magnitude of CFSE, varies with r^{-5}, r being the cation-anion distance (Burns 1993). However, the Coulomb potential, which in a simple ionic model provides most of the bonding energy, varies only with r^{-1}. If one considers the partitioning of trace elements between similar sites in various minerals, the differences in bonding energies are relevant rather than the total bonding energy. These differences, however, are dominated by CFSE, as the CFSE is much more strongly affected by subtle changes in bond lengths than the Coulomb potential. In reality, the interaction between a transition metal ion and the surrounding anions is never purely ionic. A model that can account for both mostly ionic and strongly covalent bonding effects is molecular orbital (MO) theory (Figgis 1966; Huheey 1983; Greenwood and Earnshaw 1984). In the simplest model, which considers only σ-bonding interactions, the spectroscopically ob-

TABLE 5. Crystal-field spectrum of $(Mg_{0.82}Ni_{0.18})_3Al_2(SiO_4)_3$ garnet

Band position (cm^{-1})	ϵ [L/(mol·cm)]	Excited state	Barycenter of split bands (cm^{-1})	Calc. band position (cm^{-1})
4070	8.02	$^3T_{2g}(F)$		3520
6210	10.97	$^3A_{2g}(F)$		7730
13630	1.48	$^1E_g(D)$, $^1T_{2g}(D)$		
19880	12.66	$^3T_{1g}(P)$	20640	19030
21400	11.81			

Note: Term symbols for undistorted cubic environment are used. Ground state is $^3T_{1g}(F)$. Positions of the spin-allowed bands are calculated from the crystal-field parameters in Table 6; ϵ = molar extinction coefficient of Ni in garnet as measured at the respective wavenumber.

tained crystal-field splitting measures the energy separation between the lowest antibonding and the nonbonding orbitals. This energy separation becomes larger as the overlap between the ligand and metal orbitals becomes stronger. Because bond strength increases with orbital overlap, Δ and CFSE are measures of bond strength. If π interactions between ligand and metal are considered, the picture becomes slightly more complicated, as the nonbonding orbitals of the transition metal ion now become weakly bonding or antibonding. However, because these π bonds are commonly weaker than σ bonds, the basic interpretation of Δ and CFSE as measures of bond strength is still valid.

The CFSE of 3370 cm^{-1} for Ni^{2+} in the dodecahedral site of garnet (Table 6) is exceptionally low in comparison with that of other minerals of the upper mantle: In olivine, the CFSE of Ni^{2+} in the M1 site is about 9500 cm^{-1}, and the CFSE values of Ni^{2+} in the M1 site of enstatite and diopside are 8280 and 10800 cm^{-1}, respectively (Burns 1985). This explains why the garnet-olivine partition coefficient of Ni^{2+} is very low, between 0.1 and 0.001 in the temperature range between 600 and 1600 °C (Griffin et al. 1989; Canil 1994). The CFSE of Co^{2+} in garnet, on the other hand, is only slightly lower than the values for the M1 site of enstatite (6700 cm^{-1}), diopside (6420 cm^{-1}; Burns 1985), and probably olivine. Therefore, the garnet-olivine and garnet-pyroxene partition coefficients of Co^{2+} should be close to unity, as is observed (Matsui and Banno 1969; Bodinier et al. 1987). This means that garnet in equilibrium with upper-mantle minerals should strongly fractionate Ni^{2+} from Co^{2+}. Moreover, large-scale crystallization of majorite garnet from an early magma ocean would have greatly increased the Ni/Co ratio in the remaining mantle.

Because the crystal field in the large site of the perovskite structure is similar to the dodecahedral site in garnet, some predictions on the partitioning of Ni and Co in the lower mantle are possible. Our results suggest that the CFSE of Ni^{2+} in perovskite and majorite is smaller than in magnesiowüstite (10200 cm^{-1}, Burns 1985), which means that Ni^{2+} should strongly partition in favor of magnesiowüstite. This effect should be much less pronounced for Co^{2+}. Recent experimental results by Guyot et al. (1994) are in agreement with this prediction.

TABLE 6. Crystal-field parameters of Ni^{2+} and Co^{2+} in the distorted cubic site of garnet

	Δ (cm^{-1})	B (cm^{-1})	$\beta = B/B_0$	CFSE (cm^{-1})
Co^{2+}	4430	890	0.79	5320
Ni^{2+}	4210	1080	1	3370

Note: The Δ = crystal-field splitting; B = Racah parameter; β = nephelauxetic parameter; B_0 = Racah parameter of the free ion in vacuum (B_0 = 1120 cm^{-1} for Co^{2+}; B_0 = 1080 cm^{-1} for Ni^{2+}; Figgis 1966).

ACKNOWLEDGMENTS

We thank Hubert Schulze for sample preparation and Detlef Krauße for microprobe analyses. Reviews by Bob Downs and Dave Sherman improved the manuscript.

REFERENCES CITED

Bodinier, J.-L., Dupuy, C., Dostal, J., and Merlet, C. (1987) Distribution of trace transition elements in olivine and pyroxenes from ultramafic xenoliths: Application of microprobe analysis. American Mineralogist, 72, 902–913.

Burns, R.G. (1985) Thermodynamic data from crystal field spectra. In Mineralogical Society of America Reviews in Mineralogy, 14, 277–316.

——— (1993) Mineralogical applications of crystal field theory (2nd edition), 551 p. Cambridge University Press, Cambridge.

Canil, D. (1994) An experimental calibration of the "nickel in garnet" geothermometer with applications. Contributions to Mineralogy and Petrology, 117, 410–420.

Figgis, B.N. (1966) Introduction to ligand fields, 351 p. Wiley, New York.

Gibbs, G.V., and Smith, J.V. (1965) Refinement of the crystal structure of synthetic pyrope. American Mineralogist, 50, 2023–2039.

Greenwood, N.N., and Earnshaw, A. (1984) Chemistry of the elements, 1542 p. Pergamon, Oxford, U.K.

Griffin, W.L., Cousens, D.R., Ryan, C.G., Sie, S.H., and Suter, G.F. (1989) Ni in chrome pyrope garnets: A new geothermometer. Contributions to Mineralogy and Petrology, 103, 199–202.

Guyot, F., Malavergne, V., O'Neill, H.St.C., von Seckendorf, V., Peyronneau, J., and Poirier, J.P. (1994) High-pressure transformations of iron, nickel and cobalt bearing olivines: An experimental investigation. Fifth International Symposium on Experimental Mineralogy, Petrology and Geochemistry, Abstract Supplement 1 to Terra Nova, 6, 21.

Hamilton, W.C. (1965) Significance tests on the crystallographic R factor. Acta Crystallographica, 18, 502–510.

Hazen, R.M., and Finger, L.W. (1982) Comparative crystal chemistry, 231 p. Wiley, New York.

Huheey, J.E. (1983) Inorganic chemistry (3rd edition), 936 p. Harper and Row, New York.

Keppler, H. (1992) Crystal field spectra and geochemistry of transition metal ions in silicate melts and glasses. American Mineralogist, 77, 62–75.

Keppler, H., and Rubie, D.C. (1993) Pressure-induced coordination changes of transition-metal ions in silicate melts. Nature, 364, 54–56.

Matsui, Y., and Banno, S. (1969) Partition of divalent transition metals between coexisting ferromagnesian minerals. Chemical Geology, 5, 259–265.

Novak, G.A., and Gibbs, G.V. (1971) The crystal chemistry of the silicate garnets. American Mineralogist, 56, 791–825.

Ohashi, H., Fujita, T., and Osawa, T. (1981) Structure of $Co_3Al_2Si_3O_{12}$ garnet. Journal of the Japanese Association of Mineralogists, Petrologists, and Economic Geologists, 76, 58–60.

Shannon, R.D. (1976) Revised effective ionic radii and systematic studies of interatomic distances in halides and chalcogenides. Acta Crystallographica, A32, 751–767.

Skinner, B.J. (1956) Physical properties of end-members of the garnet group. American Mineralogist, 41, 428–436.

Stahl-Brada, R., and Low, W. (1959) Optical spectrum of Co^{2+} in the cubic crystalline field of CaF_2. Physical Review, 113, 775–780.

Thibault, Y., and Walter, M.J. (1995) The influence of pressure and temperature on the metal-silicate partition coefficients of nickel and cobalt in a model C1 chondrite and implications for metal segregation in a deep magma ocean. Geochimica et Cosmochimica Acta, 59, 991–1002.

Manuscript received July 11, 1994
Manuscript accepted September 26, 1995